NASA TECHNICAL
MEMORANDUM

NASA TM X-67950

NASA TM X-67950

A MODEL FOR THE ACOUSTIC IMPEDANCE OF A PERFORATED PLATE LINER WITH MULTIPLE FREQUENCY EXCITATION

by Edward J. Rice
Lewis Research Center
Cleveland, Ohio

The effect of steady grazing flow on the liner is included in the model. Sample calculations of liner acoustic resistance with spectral excitation both with and without grazing flow are presented.

SYMBOL LIST

A_K amplitude of Kth frequency component of P_o, lbf/ft^2

b resonator cavity depth, ft

B_K amplitude of Kth frequency component of v_o, ft/sec

C speed of sound, ft/sec

C_K coefficient of Fourier cosine series fit to v_o, ft/sec

d orifice diameter, ft

L orifice effective length, ft

ℓ orifice length (perforated plate thickness), ft

M grazing flow Mach number

P_o excitation pressure at orifice, lbf/ft^2

P_K K^{th} frequency component of P_o (peak amplitude), lbf/ft^2

Q grazing flow effect on specific acoustic resistance of an orifice (eq. (11))

R_o total orifice resistance, lbm/ft^2 sec

R_{on} nonlinear orifice resistance, lbm/ft^2 sec

SPL sound pressure level (ref. 2×10^{-4} microbars)

S_K coefficient of Fourier sine series fit to v_o, ft/sec

t time, sec

t_1, t_2 initial and final time over which Fourier series fit to v_o is made (see eqs. (19) and (20)), sec

v_o orifice fluid particle velocity, ft/sec

v_{RMS} root-mean-square orifice particle velocity, ft/sec

v_∞ steady flow grazing velocity past liner, ft/sec

X_m maximum fluid displacement in orifice, ft

X_o fluid displacement in orifice, ft

δ_K phase angle for K^{th} frequency component of P_o, rad

ε orifice end correction, ft

θ specific acoustic resistance of an array of resonators

θ_o specific acoustic resistance in orifice ($\theta_o = \sigma\theta$)

θ_{of} frequency dependent part of θ_{OL} (eqs. (15) and (16))

θ_{OK} specific acoustic resistance of the Kth frequency component of P_o in the orifice

θ_{OL} linear specific acoustic resistance in orifice

θ_{ON} nonlinear specific acoustic resistance in orifice

θ_{OS} frequency independent part of θ_{OL} (eq. (14))

θ_{REF} specific acoustic resistance of an array of resonators at the fundamental frequency when the harmonic is at much lower amplitude

μ dynamic gas viscosity, lbm/ft-sec

ν kinematic gas viscosity, ft^2/sec

ρ gas density, lbm/ft^3

σ resonator array open area ratio (orifice area/wall area)

ϕ_K phase angle of Kth frequency component of v_o, rad

χ specific acoustic reactance of an array of resonators

χ_o specific acoustic reactance in orifice ($\chi_o = \sigma\chi$)

χ_{OK} specific acoustic reactance of the Kth frequency component of P_o in the orifice

ω angular frequency, rad/sec

RESONATOR IMPEDANCE MODEL

The geometry of the model and the important dimensions are shown in figure 1. The model which will be presented approximates the actual fluid motion with simplified one-dimensional flow equations.

The fluid motion between stations 0 and 1 is considered to be only mass reactance (inductive) and resistance controlled. Some of the dissipation actually occurs outside of the orifice in the jets formed by the flow (ref. 3), but the resistance is considered in the equations of the orifice since nonlinear resistance can be related to orifice velocity.

The mass continuity equation describes the conditions between stations 1 and 2. Where a relationship between pressure and density is required, the isentropic relation is used. For the calculations presented in this paper the back cavity (2 to 3) was divided into four equal segments with both mass reactance (inductance) and stiffness reactance (capacitance) considered. In this way the acoustic transmission line properties of the back cavity could be approximated without actually calculating a finite difference solution using incremental cavity lengths. In the equations which follow, however, lumped stiffness in the cavity is assumed to keep the equations simple for purposes of illustration.

When the system of equations are combined the results are:

$$\rho L \frac{d^2 X_o}{dt^2} + R_o \frac{dX_o}{dt} + \frac{\rho C^2_\sigma}{b} X_o = P_o \tag{1}$$

and

$$v_o = \frac{dX_o}{dt} \tag{2}$$

The effective length (L) of the orifice is given by:

$$L = \ell + \epsilon \tag{3}$$

where ϵ is the orifice end correction (ref. 11):

$$\epsilon = \frac{0.85\ d(1 - 0.7\ \sqrt{\sigma})}{1 + 305M^3} \tag{4}$$

The coefficient of the second derivative is associated with the inductance and that of the first derivative with the resistance of the system. The capacitance is associated with the coefficient of the displacement. The subscript on X and P denotes that they are the displacement and pressure in the orifice.

When solutions of equation (1) are considered it should be noted, as previously stated, that the more complicated system approximating wave travel in the back cavity will be used.

If the resistance R_o in equation (1) were a constant, the pressure could be given as a series of sinusoidal functions and a closed form solution would result. However, it is of interest here to consider a nonlinear

resistance term which will be considered to be a function of the orifice velocity (v_o) and displacement (X_o) as well as the grazing flow velocity (v_∞). The solution must thus be obtained by numerical integration.

The definition of the nonlinear resistance will now be developed.

Effect of Orifice and Grazing Flow Velocities on Nonlinear Resistance

The nonlinear resistance of an orifice has been shown to depend upon the magnitude of the orifice velocity (refs. 4, 5, and 6). This resistance can be written as:

$$R_{ON} = \rho |v_o| \tag{5}$$

A proportionality constant is often used to account for the effects of a discharge coefficient; however, this will not be used here.

It is convenient to use the normalized or specific resistance defined as:

$$\theta_{ON} = \frac{R_{ON}}{\rho C} = \frac{|v_o|}{C} \tag{6}$$

which is just the magnitude of the Mach number in the orifice.

The influence of a grazing flow velocity on steady flow orifice resistance can be seen in figure 2 in which the steady flow resistances of several orifices are presented both with and without grazing flow. This data is presented through permission of Pratt and Whitney Aircraft and the Boeing Company who jointly obtained this data. The steady flow resistance data will be used to develop an acoustic resistance model by equating the instantaneous acoustic resistance to the steady flow resistance.

It can be seen in figure 2 that when $v_\infty = 0$ the data can be approximated by the solid lines which are given by equation (6). This is true for both positive and negative orifice velocity. However, when a grazing flow velocity is present the results change substantially.

Three regimes can be identified which depend upon the sign and magnitude of the orifice velocity (v_o). When $v_o \geq 0$, θ_{ON} appears to be increased by a constant amount which is proportional to v_∞. This remains true for all values of positive v_o shown. For negative v_o, however, there are two regimes. There is a transition region in which θ_{ON} is approximately constant with v_o and proportional to v_∞. At sufficiently large negative values of v_o, θ_{ON} is again approximated by the solid line given by equation (6).

The equations used to describe these regions can be expressed as follows:

If $v_o \geq 0$

$$\theta_{ON} = \frac{v_o}{C} + Q \tag{7}$$

where

$$Q = 0.3 \frac{v_\infty}{C} \tag{8}$$

if $v_o < 0$

$$\theta_{ON} = Q \qquad \left(\text{for} \quad Q > \frac{|v_o|}{C} \right) \tag{9}$$

$$\theta_{ON} = \frac{|v_o|}{C} \qquad \left(\text{for} \quad Q < \frac{|v_o|}{C} \right) \tag{10}$$

As can be seen from the data in figure 2 the intercept of the dashed lines with the ordinate at $v_o = 0$ should be considered to be a function of open area ratio (σ). The definition of Q in equation (8) was thus further modified to be:

$$Q = 0.3 \frac{v_\infty}{C} \left(\frac{3.15 \times 10^{-2}}{\sigma} + 1.77 \, \sigma + 0.3 \right) \tag{11}$$

The relationships of equations (7), (9), and (10) were assumed to hold instantaneously and modified forms to account for orifice displacement were used to define the nonlinear resistance needed in equation (1).

The modified forms will now be presented.

The Effect of Displacement in the Orifice on Nonlinear Resistance

Measurements of acoustic impedance of perforated plates with single frequency sinusoidal excitation show that the resistance given by equation (6) is not attained at high frequencies. Although the fluid velocity is sufficiently high to provide a nonlinear resistance, the fluid displacements are low at high frequency.

The modification of the nonlinear resistance to account for fluid displacement might be justified by the following argument. The nonlinear dissipation is usually attributed to the energy lost in the jets formed by high amplitude oscillations (ref. 3). Unless the displacement of fluid within the orifice is sufficiently large the jet will not fully form and the amount of nonlinear dissipation (and thus resistance) will

be reduced. It was thus assumed that the fluid must be displaced a portion of the orifice diameter before a jet is fully formed. The axial extent of the turbulent mixing region can be related to the orifice diameter and thus provides the incentive to use the diameter as a normalizing factor.

The modification of equation (6) required to agree with experimental results is given by the following equation.

$$\theta_{ON} = \frac{|v_o|}{C} \, e^{-\left(\frac{d}{X_m - X_o}\right)^2} \tag{12}$$

Equation (12) is applied instantaneously in the numerical integration. The quantity X_m is the maximum displacement obtained during a cycle. This is the displacement obtained when the orifice slug comes to rest and starts to move in the opposite direction. The exponential in equation (12) is seen to act as an on-off function applied to the nonlinear resistance. When the displacement from maximum is much less than the orifice diameter (d), then $\theta_{ON} = 0$. For $(X_m - X_o) \gg d$, $\theta_{ON} \approx |v_o|/C$. The exponential in equation (12) was derived from one set of resistance versus frequency data. The justification for its use is provided by an adequate fit to a wide range of data.

It should be noted that the orifice fluid displacement correction was not applied to the grazing flow term (Q) in equations (7) to (10) but only to the $|v_o|/C$ terms.

Linear Resistance

For very small pressure amplitudes the acoustic resistance is determined by the viscous losses in the orifice. This may be accounted for by:

$$\theta_{OL} = \theta_{OS} + \theta_{of} \tag{13}$$

The steady flow resistance θ_{OS} is included to provide a low frequency limit for θ_{OL} and is given by:

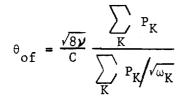$$\theta_{OS} = 5.4 \times 10^4 \, \mu \ell \tag{14}$$

where ℓ is in feet. Equation (14) was derived from a correlation given in reference 7.

For single frequency sinusoidal excitation the frequency dependent component of θ_{OL} is given by:

$$\theta_{of} = \frac{\sqrt{8\nu\omega}}{C} (1 + \ell/d) \tag{15}$$

When multiple frequency excitation is used a derived form of equation (15) can be given by

$$\theta_{of} = \frac{\sqrt{8\nu}}{C} \frac{\sum\limits_{K} P_K}{\sum\limits_{K} P_K / \sqrt{\omega_K}} \tag{16}$$

Where the P_K are the several peak pressure amplitudes. Equation (16) is not a particularly satisfactory expression for the linear resistance, but it is all that was available. What is needed is an approximate solution to the boundary layer equations of a flat plate with arbitrary motion which would replace the sinusoidal motion result of equation (16). Fortunately, the linear resistance terms are usually insignificant when compared to the nonlinear resistance terms especially when grazing flow is considered.

Equation (13) (using eq. (14) and (16)) is added to the nonlinear resistance to provide the total resistance for use in equation (1).

CALCULATION PROCEDURE

The forcing function (pressure P_o) in equation (1) can be an arbitrary function of time. However, it will be useful for the acoustic impedance calculations to describe P_o by:

$$P_o = \sum_{K} A_K \sin(\omega_K t + \delta_K) \tag{17}$$

where ω_K and A_K are chosen to simulate the desired acoustic power spectrum. Since phase information is usually not available, the phase angles (δ_K) are selected randomly.

Equations (1) and (2) are then numerically integrated using the Runge-Kutta method (ref. 8). The initial conditions are that velocity and displacement are zero. The numerical solution is allowed to progress for sufficient time for the transient solution to decay. A Fourier series fit to the calculated velocity is then started and subsequently monitored at multiples of the period of the lowest frequency component. The orifice velocity can be expressed as:

$$v_o(t) = \sum_{K} (C_K \cos \omega_K t + S_K \sin \omega_K t) \tag{18}$$

with the same frequency components considered as in equation (17). The Fourier series fit over an arbitrary time internal with frequency components which are not necessarily multiples of a fundamental is more complicated than the standard series fit. The results are the same, however, if a sufficiently long time interval is considered. This can be shown by the following expressions for the coefficients:

$$C_K = \frac{2 \int_{t_1}^{t_2} v_o(t)\cos \omega_K t \, dt + F(\omega_j t, C_j, S_j)}{(t_2 - t_1)} \tag{19}$$

and

$$S_K = \frac{2 \int_{t_1}^{t_2} v_o(t)\sin \omega_K t \, dt + G(\omega_j t, C_j, S_j)}{(t_2 - t_1)} \tag{20}$$

The ratios of the integrals to $(t_2 - t_1)$ will reach finite limits as $(t_2 - t_1) \to \infty$. The functions F and G, however, are purely oscillatory in nature and the limit of F or G divided by $(t_2 - t_1)$ will approach zero.

Once the Fourier coefficients C_K and S_K are determined the velocity can be expressed in a more convenient form as:

$$v_o(t) = \sum_K B_K \sin(\omega_K t + \phi_K) \tag{21}$$

which is an alternate form of equation (18) with phase and amplitude given by:

$$\phi_K = \text{arc } \tan\left(\frac{C_K}{S_K}\right) \tag{22}$$

and

$$B_K = \sqrt{S_K^2 + C_K^2} \tag{23}$$

Using the familiar equation for acoustic impedance as pressure divided by velocity there results

$$\theta_{OK} = \frac{A_K}{\rho C B_K} \cos(\delta_K - \phi_K) \tag{24}$$

and

$$\chi_{OK} = \frac{A_K}{\rho C B_K} \sin(\delta_K - \phi_K) \qquad\qquad (25)$$

Equations (24) and (25) express the specific acoustic resistance and reactance for the Kth frequency component in the resonator orifice. These can be converted to resonator array values for comparison with experimental data by dividing each by the open area ratio (σ) of the array.

COMPARISON WITH EXPERIMENTS

This model was developed to provide acoustic impedance calculations when the exciting pressure contains a multitude of frequency components. Unfortunately no such data exists at this time for a direct comparison. There is a small amount of two frequency data available and a comparison with this data will be made. Single frequency data currently exists which will be used to check the analytical model for the effects of orifice fluid velocity and displacement and also grazing flow velocity.

Single Frequency Without Grazing Flow

Specific acoustic resistance data obtained by Garrison (ref. 9) using the two-pressure measurement method are shown in figure 3. The data are for four samples at several frequencies with a constant sound pressure level (160 dB). The data represented by circles (ℓ = 0.05 in.) were used to derive the fluid displacement dependence expressed in equation (12). Two calculated resistance curves are shown for this condition at high frequencies with and without the displacement correction. The need for such a correction is apparent from figure 3. The comparisons with other orifice lengths (sheet thickness ℓ) is also seen to be good. The maximum errors occur with ℓ = 0.2 inch for which the data appears to be out of progression with the rest of the data at the lower frequencies.

More data from Garrison (ref. 9) are shown in figure 4. A wide range of open area ratios (σ = 0.015 to 0.13) and sound pressure levels (SPL = 130 to 168 dB) are included. The comparisons with the calculated resistances are seen to be good. Where differences occur there does not seem to be a consistent pattern with open area ratio or sound pressure level and these errors may well be within the accuracy of such measurements.

In figure 5 the specific acoustic reactances are shown for four samples (ref. 9). Again the agreement with the calculated results is considered adequate.

Single Frequency with Grazing Flow

Specific acoustic impedance measurements made by Garrison (ref. 9) are shown in figure 6. Two liner samples at two sound pressure levels were investigated using the two pressure method with grazing flow. The data at $v_\infty = 0$ are questionable since the electro-pneumatic driver provided substantial air flow which had to be bled off before reaching the sample and circulating flows resulted (conversation with Garrison).

For both samples, at the lower sound pressure level (150 dB) and high velocities, the resistance data is increasing with v_∞ indicating that the grazing flow effects are beginning to dominate the resistance. In this region the calculated results are in excellent agreement with the data. For lower values of v_∞ (especially for the $\sigma = 0.0272$ sample at 150 dB and the $\sigma = 0.0212$ sample at 160 dB) the calculated resistance underpredicts the data which are virtually flat with changing v_∞.

A possible explanation for the deviation between the data and the calculations at low grazing flow velocities can be made. Only in the case of $\sigma = 0.0272$ (160 dB) did the orifice effective length, inferred from the data, resemble that of the model (eqs. (3) and (4)). For the other data the effective length decreased much more rapidly with v_∞. In fact it dropped below the physical orifice length (ℓ) which is not allowed by the present model. The reactance was thus dropped from a fairly high positive value toward the sample tuned point ($\chi = 0$). The nonlinear resistance would then increase since $|v_0|$ is roughly proportional to $(\theta_0^2 + \chi_0^2)^{-1/2}$. The current model is unable to account for this large change in orifice effective length. This is an apparent weakness in the model which will be resolved only with the testing of a more refined instantaneous effective orifice length assumption and perhaps the study of more data.

In the regime of lower sound pressure levels and high v_∞ (of practical interest in turbofan suppressors) the agreement between the data and the theory as shown in figure 6 is quite promising.

Two Frequency Results

The results of two frequency resistance measurements made by Garrison (ref. 1) for two liner samples are shown in figure 7. This data was taken as follows. The amplitude of the fundamental frequency (2000 or 2200 Hz) was held constant at 135 decibels. The amplitude of the harmonic was then varied from 110 to 150 decibels and the impedance at the fundamental was measured. The resistance ratio was then formed with θ_{REF} being the resistance at the fundamental frequency for low harmonic amplitude ($\approx$110 dB).

Calculated resistance values were obtained under the same conditions. Qualitative agreement is seen between the theory and the data in that the

second harmonic amplitude, at high amplitude, determines the resistance at the fundamental frequency. To produce agreement between theory and data, the second harmonic amplitude must be about 4 or 5 decibels higher in the calculation for one sample ($\sigma = 0.054$) and about 10 dB higher for the other ($\sigma = 0.08$). It is also disappointing that the trends (amplification of resistance by the harmonic) between the two samples is opposite in the data to that in the theory.

It is not obvious what changes in the theory would be required to get agreement with the two frequency data without destroying the excellent agreement that was obtained with the single frequency data. It is also not obvious that the theory should be altered on the basis of this small amount of data.

A calculated result of Groeneweg (ref. 10) is also shown in figure 7. This uses overall sound pressure level for the two frequencies applied to a single frequency model as in reference 11. This method overpredicts the interaction effect since it essentially applies the entire harmonic pressure amplitude to the fundamental frequency impedance calculation.

The agreement between theory and experiment is not at this time completely satisfactory. However, it is not clear which is at fault until additional data is thoroughly investigated. The interaction effect of one frequency upon another is clearly demonstrated to be of importance by both the theory and experimental data.

SAMPLE CALCULATIONS WITH SPECTRAL EXCITATION

The exciting pressure spectra used in the sample calculations are shown in figure 8(a). Six pressure terms (for use in eq. (1)) are used with a constant sound pressure level of 130 decibels. These are spaced at 500 Hz intervals and are intended to provide a crude simulation of white noise. The phases are chosen randomly. At 1875 Hz a pressure component is used with its amplitude varying from 130 to 150 decibels. This component is intended to simulate a discrete tone standing at or above the white noise. Hereafter these simulations will be referred to as the white noise and the discrete tone.

In figure 8(b) some sample calculations of specific acoustic resistance (θ) with zero grazing flow velocity ($v_\infty = 0$) are shown. The interaction effect of the discrete tone with the background white noise is clearly demonstrated. When the discrete tone is at the same level as the white noise (130 dB), the resistance spectrum is fairly flat with values around $\theta = 0.25$. When the discrete tone is increased to 140 dB the resistance at the white noise frequencies increases to about 0.5 and at 150 dB to about 1.1. An interesting observation in figure 8(b) is that the resistances at the white noise frequencies are increased more than the resistance at the discrete tone frequency itself. This appears to be a general trend for the limited number of sample calculations completed thus far.

In figure 9 the same pressure spectrum as shown in figure 8(a) is applied to the acoustic liner but this time with a grazing flow velocity of $v_\infty = 400$ feet per second. Here the resistance is mainly grazing flow dominated and the amplitude of the discrete tone has much less effect. Only at the highest discrete tone amplitude (150 dB) are the resistances at the white noise frequencies increased and then only by a small amount. Again the resistances at the white noise frequencies are increased more than at the discrete tone.

Small irregularities in θ with frequency should not be considered as significant since the resistances are somewhat effected by the choice of pressure phase angles. This is demonstrated in figure 10 where three choices of phase angles were used both with and without grazing flow. The phase angles were still chosen at random, but three different random sets were used. The variations with phase angle are not large, but perhaps an average should be used over several sets of phase angle choices to better define the resistance. This will have to be done since phase information is usually lacking.

CONCLUDING REMARKS

Several investigators have used a single frequency sinusoidal excitation impedance model in an attempt to model an acoustic linear with spectral excitation (refs. 11 to 13). Two methods have been used to modify these models to account for the multiple frequency excitation.

The first method uses the overall sound pressure level of the noise spectrum (refs. 11 and 12). This results in applying the same pressure amplitude at each frequency. Since the reactance varies with frequency and helps determine the peak orifice particle velocity, the nonlinear resistance at each frequency will be different. This method results in a low resistance at both high and low frequencies with a maximum at the liner tuned frequency ($\chi = 0$).

The second method as used in reference 13 and discussed in reference 11 uses a root-mean-square particle velocity (v_{RMS}) approach. A peak orifice particle velocity is calculated at several frequencies using the sound pressure level at each frequency. Then v_{RMS} is formed from the several velocities to give a single velocity to represent the spectrum. This root-mean-square velocity is used in an equation similar to equation (5) (or an equation derived from expressions like eqs. (7) to to (10) if v_∞ were considered) to calculate resistance. Thus the resistance spectrum is uniform with frequency.

From the preliminary calculations presented in this paper in figures 8(b), 9, and 10 the resistance spectrum appears to be fairly uniform with the possible exception of the frequencies at which the high amplitude discrete tone appears. This uniformity suggests that the v_{RMS} method is at least qualitatively more correct than the overall sound pressure level method.

More extensive sample calculations will have to be studied to supplement the preliminary calculations of this paper. Of particular interest will be a more thorough investigation of the minimum resistance obtained at the high amplitude discrete tone in figure 8(b).

CONCLUSIONS

A model has been presented which can be used to calculate acoustic impedance of a perforated plate liner which is excited by multiple frequencies. The nonlinear interaction effects of this spectral excitation can be calculated simultaneously with the effects of grazing flow velocity and orifice fluid velocity and displacement. The results of the calculations have shown the following.

1. When the model is reduced to single frequency excitation, it provides acceptable agreement with experimental data for variations in sound pressure level, grazing flow, and frequency.

2. When the model is used with two frequency excitation a strong interaction of the amplitude at one frequency upon the resistance at the other frequency is observed. This effect is not as great as a very limited amount of experimental data would indicate. Final judgment cannot be made as to which is correct until more data are thoroughly investigated.

3. Sample impedance calculations were made with a strong discrete tone superimposed upon a simulated white noise spectrum. The acoustic resistances at all frequencies were found to increase dramatically with increasing discrete tone sound pressure level when there was no grazing flow. However, with the presence of a 400 feet per second grazing flow, increasing discrete tone amplitude had only a small effect upon acoustic resistance.

4. With spectral excitation the acoustic resistance was found to be fairly uniform with frequency. A possible exception was observed at the frequency of the strong discrete tone where the resistance appears to be lower than at the other frequencies.

5. The choice of phase relationships between the several frequencies of excitation appears to have only a small effect on the impedance calculations.

REFERENCES

1. G. D. Garrison; A. C. Schnell; and C. D. Baldwin, Pratt & Whitney Aircraft Rep. PWA-FR-3210 (1969).

2. L. S. Wirt, Presented at the Acoustical Society of America Meeting, Washington, D.C. (Apr. 20-23, 1971).

3. U. Ingard, and S. Labate, J. Acoust. Soc. Am. <u>22</u>, 211-218 (1956).

4. U. Ingard, and H. Ising, J. Acoust. Soc. Am. <u>42</u>, 6-17 (1967).

5. B. T. Zinn, AIAA Paper 69-481 (1969).

6. W. A. Sirignano, and T. S. Tonon, Princeton Univ. Rep. AMS-SR-553-h, NASA CR-72426 (1968).

7. M. D. Nelsen, B. A. Linscheid, B. A. Dinwiddie, and O. J. Hall, Boeing Co. Rep. D3-8535 (1971).

8. J. B. Scarborough, <u>Numerical Mathematical Analysis</u> (The Johns Hopkins Press, Baltimore, 1962), 5th ed.

9. G. D. Garrison, A. C. Schnell, C. D. Baldwin, and P. R. Russell, Pratt & Whitney Aircraft Rep. PWA-FR-3299 (1969).

10. J. F. Groeneweg, NASA SP-207, 357-368 (1969).

11. E. J. Rice, C. E. Feiler, and L. W. Acker, NASA TN D-6178 (1971).

12. J. F. Groeneweg, C. E. Feiler, and L. W. Acker, NASA TN D-6395 (1971).

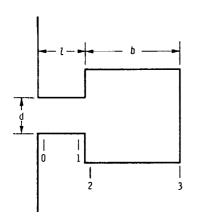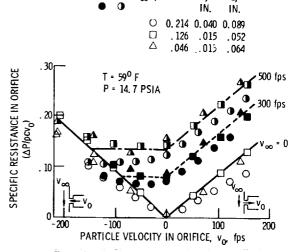13. W. Eversman, M. D. Nelson, D. Armstrong, and O. J. Hall, AIAA Paper 71-731 (1971).

Figure 1. - Geometry used in analytical model.

Figure 2. - Steady flow specific resistance in the orifice as a function of orifice velocity (v_0) and grazing flow velocity (v_∞). Data obtained by Pratt & Whitney and the Boeing Company.
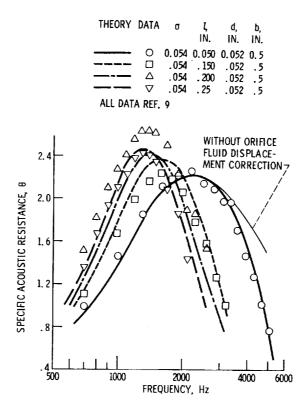

Figure 3. - Specific acoustic resistance, comparison of theory and experiment at constant sound pressure level (160 dB).
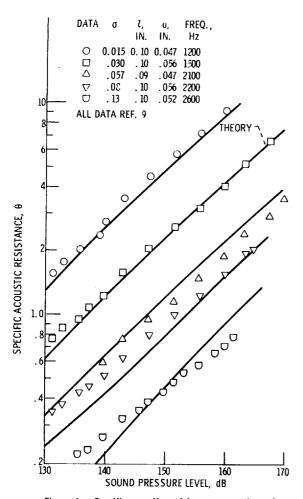
Figure 4. - Specific acoustic resistance, comparison of theory and experiment at varying sound pressure level.
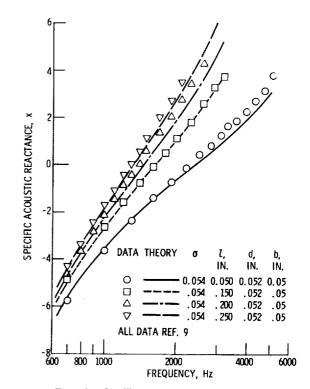
Figure 5. - Specific acoustic reactance, comparison of theory and experiment at constant sound pressure level (160 dB).
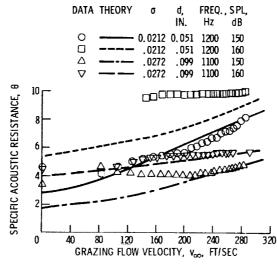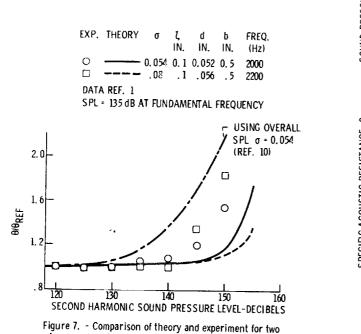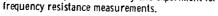
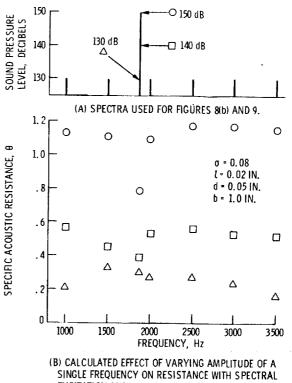Figure 6. - Specific acoustic resistance, comparison of theory and experiment with varying grazing flow velocity, v_∞.

EXP.	THEORY	σ IN.	ℓ IN.	d IN.	b IN.	FREQ. (Hz)
○	——	0.054	0.1	0.052	0.5	2000
□	- - -	.08	.1	.056	.5	2200

DATA REF. 1

SPL = 135 dB AT FUNDAMENTAL FREQUENCY

┌ USING OVERALL
  SPL σ = 0.054
  (REF. 10)

θ/θ_REF

SECOND HARMONIC SOUND PRESSURE LEVEL-DECIBELS

Figure 7. - Comparison of theory and experiment for two frequency resistance measurements.

(A) SPECTRA USED FOR FIGURES 8(b) AND 9.

SOUND PRESSURE LEVEL, DECIBELS

○ 150 dB
□ 140 dB
△ 130 dB

SPECIFIC ACOUSTIC RESISTANCE, θ

σ = 0.08
ℓ = 0.02 IN.
d = 0.05 IN.
b = 1.0 IN.

FREQUENCY, Hz

(B) CALCULATED EFFECT OF VARYING AMPLITUDE OF A SINGLE FREQUENCY ON RESISTANCE WITH SPECTRAL EXCITATION AND $v_\infty = 0$.

Figure 8

DISCRETE TONE AMPLITUDE

△	130
□	140
○	150

σ = 0.08
ℓ = 0.02 IN.
d = 0.05 IN.
b = 1.0 IN.

SPECIFIC ACOUSTIC RESISTANCE, θ

PRESSURE EXCITATION SPECTRUM AS IN FIG. 8(A)
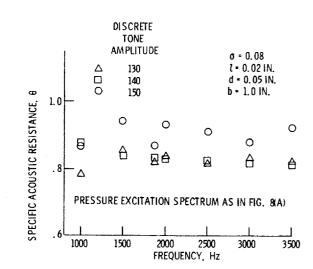
FREQUENCY, Hz

Figure 9. - Calculated effect of varying amplitude of a single frequency on acoustic resistance with spectral excitation and $v_\infty = 400$ ft/sec.

σ = 0.08
ℓ = 0.02 IN.
d = 0.05 IN.
b = 1.0 IN.

ALL SPL = 130 dB EXCEPT AT 1875 Hz WHERE SPL = 140 dB

OPEN SYMBOLS $v_\infty = 0$
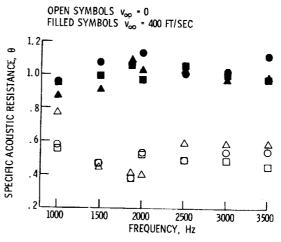FILLED SYMBOLS $v_\infty = 400$ FT/SEC

SPECIFIC ACOUSTIC RESISTANCE, θ

FREQUENCY, Hz

Figure 10. - Calculated variation of acoustic resistance with choice of phase angles for spectral pressure components.